

Cambridge Centre for Computational Chemical Engineering

University of Cambridge

Department of Chemical Engineering and Biotechnology

Preprint

ISSN 1473 – 4273

Numerical investigation of DQMoM-IEM as a turbulent reaction closure

Jethro Akroyd¹, Alastair J. Smith¹,

Laurence R. McGlashan¹, Markus Kraft¹

released: 24 June 2009

¹ Department of Chemical Engineering
and Biotechnology
University of Cambridge
New Museums Site
Pembroke Street
Cambridge, CB2 3RA
UK
E-mail: mk306@cam.ac.uk

Preprint No. 76



c4e

Key words and phrases: Mathematical modelling, Simulation, Turbulence, CFD, DQMoM-IEM

Edited by

Cambridge Centre for Computational Chemical Engineering
Department of Chemical Engineering
University of Cambridge
Cambridge CB2 3RA
United Kingdom.

Fax: + 44 (0)1223 334796

E-Mail: c4e@cheng.cam.ac.uk

World Wide Web: <http://www.cheng.cam.ac.uk/c4e/>

Abstract

This paper investigates a mean reaction rate closure for turbulent reacting flows called the Direct Quadrature Method of Moments using the Interaction by Exchange with the Mean micromixing model (DQMoM-IEM). The method is not new, but we present a systematic study that considers several important new aspects of the method. We present a rigorous numerical investigation of the behaviour and implementation of the method in a commercial computational fluid dynamics (CFD) package. The problems that arise are discussed in detail. We present practical hints and propose solutions to resolve these issues. In particular we demonstrate a new analytic expression for the DQMoM-IEM source terms. We extend the methodology to take advantage of this expression and show details of the implementation in the CFD code. We present an extensive set of numerical experiments and validation. The method is demonstrated to work for a problem known from the literature which includes an isothermal dimerisation process. Experimental and transported probability density function (PDF) data compare reasonably well. The method is discussed critically and areas for further research are suggested to make the method more practical.

Contents

| | | |
|----------|---|-----------|
| 1 | Introduction | 3 |
| 2 | Theoretical background | 5 |
| 2.1 | DQMoM | 5 |
| 2.2 | DQMoM-IEM | 6 |
| 3 | Numerical investigation | 7 |
| 3.1 | DQMoM-IEM coupling to Star-CD | 7 |
| 3.2 | DQMoM-IEM behaviour | 8 |
| 3.2.1 | Source terms | 9 |
| 3.2.2 | General solver | 11 |
| 3.2.3 | Full analytic solver | 13 |
| 4 | Numerical experiments and validation | 14 |
| 4.1 | Model problem | 14 |
| 4.2 | Solver validation | 17 |
| 4.3 | Solver application to reacting flow | 18 |
| 4.4 | Solver efficiency | 20 |
| 4.5 | Significance of the choice of boundary conditions | 21 |
| 5 | Conclusions | 22 |
| | Nomenclature | 23 |
| | References | 26 |
| | Citation Index | 29 |
| A | DQMoM derivation | 30 |
| A.1 | DQMoM | 30 |
| A.2 | DQMoM-IEM | 33 |
| B | Method of moments implementation | 34 |

1 Introduction

Turbulent reacting flows are an important field of research. The modelling of such flows is a valuable element of this research and is relevant to many engineering applications. For example, the optimisation of diesel combustion to increase fuel efficiency and reduce soot and NO_x emissions. Current turbulent flow models separate the velocity and scalar fields (for example species concentration) into resolved and unresolved fields. They solve transport equations for the resolved fields, but need to close terms arising from the unresolved fields. In reacting flows, the *chemical source term* that occurs in the material and energy balance equations is left unclosed by the unresolved fields and must be modelled.

Transported probability density function (PDF) methods offer a promising approach [18]. They are applicable to all chemistry and flows. The key advantage for reacting flows is that the chemical source term is closed by the joint composition PDF. However, the direct solution of transported PDF methods is difficult. Monte Carlo methods are typically used [18, 19]. This presents several issues. Such methods are often computationally expensive and they are not available in the existing computational fluid dynamics (CFD) software that would be the turbulent flow method of choice for many engineering calculations. Presumed PDF methods offer a related approach. They assume a functional form for the joint composition PDF based on transported low-order moments, for example the mean and variance. However, they can only be as accurate as the assumed form of the PDF. Historically, they have not been successful for non-premixed turbulent combustion [1].

Several method of moments approaches have been used to address unclosed terms that arise in population balance equations (PBEs). The method of moments with interpolative closure (MoMIC) [6, 7] closes fractional-order moments by interpolation among whole-order moments in terms arising due to coagulation and growth processes. However, this would translate to an *extrapolative* chemical source term closure and would be rendered intractable by the number of moments involved. The quadrature method of moments (QMoM) [16] uses a quadrature approximation (a weighted particle system) to close terms arising due to growth processes. The quadrature approximation is calculated from low-order moments each time it is required. QMoM was initially formulated for univariate distributions [16]. It has since been extended to a bivariate case [28].

The direct quadrature method of moments (DQMoM) [5, 15] is an extension of QMoM. It uses an arbitrary moment set to derive transport equations for the particle system. It can be applied to multiple scalars and guarantees to reproduce the transport of the moment set used in the derivation. The transport equations share the form of standard Eulerian scalar transport equations and the method is amenable to implementation within the infrastructure of existing CFD codes. The DQMoM derivation is summarised by Fox [5]. The interaction by exchange with the mean (IEM) [26] micromixing model is used and the resulting method is deterministic. A linear system must be inverted to calculate the source terms. Fox notes that the linear system is singular if any particles occupy the same location in composition space. A small perturbation of the particles is suggested in order to overcome this. It is also noted that the application of DQMoM to inhomogeneous scalar mixing is compromised by violations of boundedness. An alternative algorithm, DQMoM-IEM is suggested to address this issue. It constrains the method to use conserved weights and transport unmixed moments. Several applications have been investigated.

Fan et al. [4] and Fan and Fox [3] applied monovariate DQMoM with $N = 2, 3, 4$ particles to a PBE describing aggregation and breakage in a fluidised bed. Fan et al. [4] used a condition number to detect singularities in the source term calculation. In the singular (or near singular) case, they suggested either setting the source terms to zero, or estimating them based on neighbour cells. $N = 3$ was reported as optimal. Fan and Fox [3] reported that $N \geq 3$ was required for cases with a wide PSD and significant segregation. Zucca et al. [29] applied DQMoM to a PBE describing soot formation in turbulent flames, using a presumed beta-PDF method to close the chemical source term. Zucca et al. [30] extended this work to validate bivariate DQMoM against Monte Carlo simulations. They showed that more particles gave increased accuracy, but also greater numerical difficulties. The choice of the moment set affected accuracy and numerical stability. Lower-order moments gave better conditioning. The use of fractional moments was suggested.

Wang and Fox [27] applied DQMoM-IEM to simulate reactive-precipitation in plug-flow and report agreement with transported PDF data for $N = 2, 3, 4$ particles. They discuss the singularities in the source term calculation and describe approaches using either a perturbation method or values based on neighbour cells. They avoid violations of boundedness by not calculating the source terms where the scalars are near their theoretical bounds. A few publications have applied DQMoM-IEM with $N = 2$ particles to turbulent combustion. Raman et al. [20] reported reasonable agreement with Monte Carlo data for Large Eddy Simulations (LES) of a reacting shear layer and bluff body flame. In the flame case, a laminar flamelet chemistry model was used and the mixture fraction was transported by DQMoM-IEM. Tang et al. [22] reported similar agreement with experimental data for a Reynolds-averaged Navier Stokes (RANS) simulation of a bluff-body methane flame.

The stochastic fields (SF) [21, 25] method shares some similarities with DQMoM and is equally amenable to implementation within existing CFD codes. It uses Eulerian fields to approximate the one-point joint composition PDF. Each field contains the value of each scalar over the solution domain. This is similar to the particle description used by DQMoM. The method has been applied a number of turbulent reacting flow problems including piloted methane flames [17], the auto-ignition of hydrogen flames [12, 13] and the dispersion of reactive pollutants [10]. Each of these SF applications have used the IEM micromixing model. The key difference from DQMoM is that SF uses a stochastic solution method. A sufficient number of fields must be used to reduce statistical error.

The **purpose of this paper** is to study the numerical behaviour of DQMoM-IEM and investigate its implementation in the Star-CD [2] CFD code. DQMoM-IEM is attractive because it is deterministic such that the number of particles can be selected based on the approximation appropriate to the problem, rather than to control statistical error.

The rest of this paper is structured as follows. Section 2 introduces the key features of DQMoM and DQMoM-IEM. Section 3 presents a rigorous numerical investigation of DQMoM-IEM. A new analytic expression is presented for the DQMoM-IEM source terms. Two DQMoM-IEM solvers based on this expression and the coupling to the Star-CD [2] CFD code are discussed in detail. Section 4 validates the DQMoM-IEM solvers against the method of moments and a turbulent reaction test case known from the literature [14, 23, 24]. Issues regarding boundary conditions are discussed and areas for further investigation are suggested to make the method more practical.

2 Theoretical background

This section introduces the key features of DQMoM and DQMoM-IEM. The derivations are well documented in the literature and are described in detail by Fox [5, Appendix B].

The derivations are summarised in Appendix A for the benefit of any readers who would appreciate more detail. The derivations are presented in a general multivariate component form and may be of particular use to anyone who wishes to implement DQMoM.

2.1 DQMoM

A closed joint composition PDF transport equation

$$\frac{\partial f_\phi}{\partial t} + \langle U_i \rangle \frac{\partial f_\phi}{\partial x_i} - \frac{\partial}{\partial x_i} \left(\Gamma_T \frac{\partial f_\phi}{\partial x_i} \right) = - \frac{\partial}{\partial \psi_\alpha} \left[\left(\frac{C_\phi}{2\tau_\phi} (\langle \phi_\alpha \rangle - \psi_\alpha) + S_\alpha(\psi) \right) f_\phi \right]. \quad (1)$$

is approximated using a weighted particle system

$$\begin{aligned} f_\phi(\psi; x, t) \, \mathbf{d}\psi &= f_\phi(\psi_1, \psi_2, \dots, \psi_K; x, t) \, \mathbf{d}\psi_1 \cdots \mathbf{d}\psi_K \\ &\approx \sum_{n=1}^N w^{(n)}(x, t) \prod_{\alpha=1}^K \delta_{\psi_\alpha^{(n)}; x, t} \, \mathbf{d}\psi_\alpha^{(n)}, \end{aligned} \quad (2)$$

where

$$\delta_{\psi_\alpha^{(n)}; x, t} \equiv \delta [\psi_\alpha - \psi_\alpha^{(n)}(x, t)], \quad (3)$$

$$\sum_{n=1}^N w^{(n)}(x, t) = 1. \quad (4)$$

The system contains $N(K+1)$ unknowns comprising the weights $w^{(n)}$ and positions $\psi_\alpha^{(n)}$, where $n = 1, \dots, N$ particles and $\alpha = 1, \dots, K$ scalars in the composition vector ϕ .

Transport equations that share the form of standard scalar transport equations are derived for the weights $w^{(n)}$ and weighted positions $s_\alpha^{(n)}$ of the particle system

$$\frac{\partial w^{(n)}}{\partial t} + \langle U_i \rangle \frac{\partial w^{(n)}}{\partial x_i} - \frac{\partial}{\partial x_i} \left[\Gamma_T \frac{\partial w^{(n)}}{\partial x_i} \right] = a^{(n)}, \quad (5)$$

$$\frac{\partial s_\alpha^{(n)}}{\partial t} + \langle U_i \rangle \frac{\partial s_\alpha^{(n)}}{\partial x_i} - \frac{\partial}{\partial x_i} \left[\Gamma_T \frac{\partial s_\alpha^{(n)}}{\partial x_i} \right] = b_\alpha^{(n)}, \quad (6)$$

where

$$s_\alpha^{(n)} \equiv w^{(n)} \psi_\alpha^{(n)}. \quad (7)$$

The source terms $a^{(n)}$ and $b_\alpha^{(n)}$ are described by an algebraic linear system (equation A.16). The derivation of the linear system uses a set of $M = N(K + 1)$ empirical moments

$$\langle \phi_1^{m_{m1}} \dots \phi_K^{m_{mK}} \rangle_N = \sum_{n=1}^N w^{(n)} \prod_{\alpha=1}^K \psi_\alpha^{(n)m_{m\alpha}} \quad \text{for } m = 1, \dots, M, \quad (8)$$

to force the particle system to obey the equivalent moment transport equations that could be derived from equation (1). The correct transport of empirical moments outside this set is not certain.

Fox [5] notes that DQMoM does not guarantee boundedness of the particle positions when applied to joint PDFs defined on bounded domains. It is further noted that the linear system is often poorly conditioned and is rank deficient if any particles occupy the same location in composition space. It is implicit that this difficulty will increase as the size of the linear system increases with the number of scalars.

2.2 DQMoM-IEM

DQMoM-IEM constrains DQMoM to use particles with *conserved* weights and transport only *unmixed* moments. It is suggested by Fox [5] to ensure boundedness.

By definition, the source term of a conserved scalar is null

$$a^{(n)} = 0. \quad (9)$$

The source terms $b_\alpha^{(n)}$ are described by an algebraic linear system of NK equations. The derivation of the linear system uses $M = NK$ unmixed empirical moments

$$\langle \phi_\alpha^{m_{m\alpha}} \rangle_N = \sum_{n=1}^N w^{(n)} \psi_\alpha^{(n)m_{m\alpha}} \quad \text{for } m = 1, \dots, M. \quad (10)$$

The unmixed constraint ensures that the scalars are uncoupled [5] and the linear system may be written

$$\sum_{n=1}^N \psi_\alpha^{(n)m_{m\alpha}-1} (b_\alpha^{(n)} - w^{(n)} r_\alpha^{(n)}) = \sum_{n=1}^N (m_{m\alpha} - 1) \psi_\alpha^{(n)m_{m\alpha}-2} w^{(n)} c_{\alpha\alpha}^{(n)} \quad (11)$$

for $m = 1, \dots, M$,

where

$$c_{\alpha\beta}^{(n)} \equiv \Gamma_T \frac{\partial \psi_\alpha^{(n)}}{\partial x_i} \frac{\partial \psi_\beta^{(n)}}{\partial x_i}, \quad (12)$$

$$r_\alpha^{(n)} \equiv \frac{C_\phi}{2\tau_\phi} (\langle \phi_\alpha \rangle_N - \psi_\alpha^{(n)}) + S_\alpha(\psi^{(n)}). \quad (13)$$

DQMoM-IEM is likely to be of most interest in applications where only low-order integer moments are required. For example, in a two-particle system, the unmixed empirical moments may be specified as K means $\langle \phi_\alpha \rangle_N$ and K second moments $\langle \phi_\alpha^2 \rangle_N$.

3 Numerical investigation

The implementation of DQMoM-IEM in the Star-CD [2] CFD code and the numerical behaviour of DQMoM-IEM were considered in detail.

Section 3.1 describes an operator splitting used to couple DQMoM-IEM and Star-CD. The splitting enables the most appropriate numerical method to be applied to each part of the problem. For example, the Star-CD algebraic multigrid (AMG) method works well for conserved scalars, but not scalars with stiff source terms. For this reason, the splitting is such that the DQMoM-IEM source terms are integrated outside Star-CD.

Section 3.2 presents a new analytic expression for the source terms $b_\alpha^{(n)}$ and considers their numerical behaviour in detail. The problems that arise during the integration of the source terms are discussed and two DQMoM-IEM solvers are suggested to resolve these issues.

3.1 DQMoM-IEM coupling to Star-CD

DQMoM-IEM and Star-CD [2] are coupled using an operator splitting. The objective is to solve equations (5) and (6).

The weights $w^{(n)}$ and weighted positions $s_\alpha^{(n)}$ are set up in Star-CD as passive scalars with no source term. The transport equations (5) and (6) are rewritten as

$$\frac{\partial \varphi}{\partial t} = \mathcal{F}_1(\varphi) + \mathcal{F}_2(\varphi) , \quad (14)$$

and are integrated as a transient problem using a second-order operator splitting

$$\text{Step 1:} \quad \varphi^{\dagger 1} = \varphi(t) + \int_0^{\frac{1}{2}\Delta t} \mathcal{F}_1(\varphi) \, d\tau \quad \text{with } \varphi = \varphi(t) \text{ at } \tau = 0 , \quad (15)$$

$$\text{Step 2:} \quad \varphi^{\dagger 2} = \varphi^{\dagger 1} + \int_0^{\Delta t} \mathcal{F}_2(\varphi) \, d\tau \quad \text{with } \varphi = \varphi^{\dagger 1} \text{ at } \tau = 0 , \quad (16)$$

$$\text{Step 3:} \quad \varphi(t + \Delta t) = \varphi^{\dagger 2} + \int_0^{\frac{1}{2}\Delta t} \mathcal{F}_1(\varphi) \, d\tau \quad \text{with } \varphi = \varphi^{\dagger 2} \text{ at } \tau = 0 , \quad (17)$$

where the time step Δt is specified via Star-CD. The operators \mathcal{F}_1 and \mathcal{F}_2 are defined

$$\mathcal{F}_1(w^{(n)}) = a^{(n)} , \quad (18)$$

$$\mathcal{F}_1(s_\alpha^{(n)}) = b_\alpha^{(n)} , \quad (19)$$

$$\mathcal{F}_2(w^{(n)}) = -\langle U_i \rangle \frac{\partial w^{(n)}}{\partial x_i} + \frac{\partial}{\partial x_i} \left[\Gamma_T \frac{\partial w^{(n)}}{\partial x_i} \right] , \quad (20)$$

$$\mathcal{F}_2(s_\alpha^{(n)}) = -\langle U_i \rangle \frac{\partial s_\alpha^{(n)}}{\partial x_i} + \frac{\partial}{\partial x_i} \left[\Gamma_T \frac{\partial s_\alpha^{(n)}}{\partial x_i} \right] . \quad (21)$$

The operator splitting scheme is illustrated in Figure 1. Step 2 is implemented using Star-CD to solve conserved transport equations for each scalar. Steps 1 and 3 are called from a user-defined subroutine at the beginning and end of each Star-CD iteration. This provides a convenient way to perform each splitting step within a single iteration.

A computationally efficient coupling is achieved by combining step 3 with step 1 of the following iteration, with the obvious exception of the last iteration. The implementation may be easily run across multiple processors using the parallel features of Star-CD.

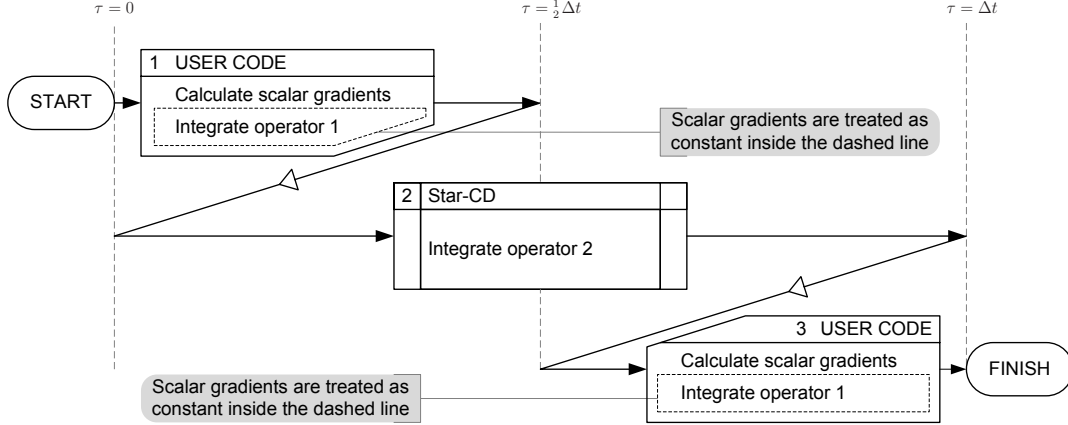


Figure 1: Operator splitting used to implement DQMoM-IEM within Star-CD.

The spatial gradients of $\psi_\alpha^{(n)}$ are required in steps 1 and 3. The gradients of the transported scalars $w^{(n)}$ and $s_\alpha^{(n)}$ are evaluated using Star-CD and the gradients of $\psi_\alpha^{(n)}$ are calculated

$$\frac{\partial \psi_\alpha^{(n)}}{\partial x_i} = \begin{cases} \frac{1}{w^{(n)}} \left(\frac{\partial s_\alpha^{(n)}}{\partial x_i} - \frac{s_\alpha^{(n)}}{w^{(n)}} \frac{\partial w^{(n)}}{\partial x_i} \right) & \text{if } w^{(n)} \neq 0 \\ 0 & \text{otherwise.} \end{cases} \quad (22)$$

In the case $w^{(n)} = 0$, the gradient is arbitrarily set to zero. A feature of Star-CD is that the gradients are evaluated simultaneously *for all cells* in a domain. It is convenient to calculate the gradients over the whole domain at the start of the step. These values are treated as constants for the remainder of step, as illustrated by the dashed lines in Figure 1. The numerical approach to the remainder of steps 1 and 3 is described in Section 3.2.

3.2 DQMoM-IEM behaviour

This section considers the numerical behaviour of DQMoM-IEM. The objective is to identify and resolve the problems that occur when integrating the set of NK ordinary differential equations (ODEs)

$$\frac{\partial s_\alpha^{(n)}}{\partial t} = b_\alpha^{(n)}, \quad (23)$$

as per steps 1 and 3 of the operator splitting (see Section 3.1, equations 15, 17 and 19).

3.2.1 Source terms

This section presents a new analytic expression for the DQMoM-IEM source terms $b_\alpha^{(n)}$ and discusses the numerical issues that arise when integrating equation (23).

The source terms are described by the algebraic linear system given in equation (11). The scalars in equation (11) are uncoupled and if the unmixed empirical moments are specified

$$m_{m\alpha} = m \quad \text{for } m = 1, \dots, N \text{ and } \alpha = 1, \dots, K. \quad (24)$$

equation (11) represents a set of N equations for each scalar $\alpha = 1, \dots, K$ and can be solved analytically to give

$$b_\alpha^{(n)} = w^{(n)} r_\alpha^{(n)} + w^{(n)} c_{\alpha\alpha}^{(n)} \sum_{\substack{i=1 \\ i \neq n}}^N \frac{1}{\psi_\alpha^{(n)} - \psi_\alpha^{(i)}} + \prod_{\substack{i=1 \\ i \neq n}}^N \frac{1}{\psi_\alpha^{(n)} - \psi_\alpha^{(i)}} \left[\sum_{\substack{j=1 \\ j \neq n}}^N w^{(j)} c_{\alpha\alpha}^{(j)} \prod_{\substack{k=1 \\ k \neq j, n}}^N (\psi_\alpha^{(j)} - \psi_\alpha^{(k)}) \right]. \quad (25)$$

The solution is constrained to the moments specified in equation (24), but is general in the sense that equation (25) may be **applied to any number of particles and scalars**. In the $N = 2$ particle case, equation (25) simplifies to

$$b_\alpha^{(1)} = \frac{w^{(1)} c_{\alpha\alpha}^{(1)} + w^{(2)} c_{\alpha\alpha}^{(2)}}{\psi_\alpha^{(1)} - \psi_\alpha^{(2)}} + w^{(1)} r_\alpha^{(1)}, \quad b_\alpha^{(2)} = \frac{w^{(1)} c_{\alpha\alpha}^{(1)} + w^{(2)} c_{\alpha\alpha}^{(2)}}{\psi_\alpha^{(2)} - \psi_\alpha^{(1)}} + w^{(2)} r_\alpha^{(2)}, \quad (26)$$

where an equivalent expression was previously given by Wang and Fox [27] for $N = 2$.

The availability of equation (25) presents two key advantages. Firstly, it negates the need to solve equation (11) numerically. Secondly, the analytic form of the source terms gives the following valuable insights into the behaviour of the system.

The term containing r_α describes the chemical reaction and micromixing processes. These will be referred to as the *reaction* and *micromixing* terms. The reaction term will likely require an implicit ODE solver. The micromixing term may be integrated numerically with the reaction term. The numerical treatment of such systems has been widely studied [11]. The presence of these terms does not pose a new challenge.

The terms containing $c_{\alpha\alpha}$ describe the effect of turbulent diffusion in the presence of spatial gradients of scalar α . They will be collectively referred to as the *diffusion* term. The diffusion term conserves the scalar means. This is demonstrated in equation (26), where the diffusion terms are equal and opposite. However, the functional form of the diffusion term presents several challenges to the DQMoM-IEM implementation.

Figure 2(a) shows the form of the diffusion and micromixing terms in an inert $N = 2$ particle system. The diffusion term produces variance by causing the particles to diverge. It is singular and discontinuous where $\psi_\alpha^{(1)} = \psi_\alpha^{(2)}$. The micromixing term causes the particles to converge. It is responsible for decay of the variance. Figure 2(b) shows the net source term and illustrates a problem. If $\psi_\alpha^{(n)}$ is defined on a bounded domain $[0, 1]$, a particle $0.8 < \psi_\alpha^{(2)} \leq 1$ has a net positive source term and will move out of bounds.

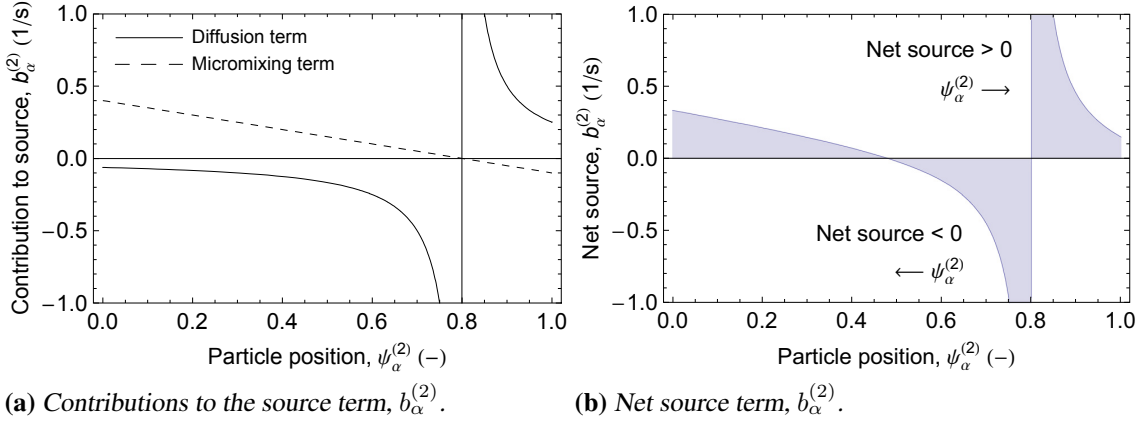


Figure 2: Functional form of the source term for an inert $N = 2$ particle system.

The source term is shown as a function of the particle position $\psi_\alpha^{(2)}$ where $\psi_\alpha^{(1)} = 0.8$, $w^{(1)} = w^{(2)} = 1/2$, $c_{\alpha\alpha}^{(1)} = 10^{-1}$ 1/s, $c_{\alpha\alpha}^{(2)} = 10^{-4}$ 1/s and $C_\phi = 2$, $\tau_\phi = 1/2$ s.

Figure 3 shows two possible forms of the diffusion term in an $N = 3$ particle system. The diffusion term is singular and discontinuous where any $\psi_\alpha^{(n)}$ are equal. The difference between Figure 3(a) and 3(b) is due to the relative magnitude of the $c_{\alpha\alpha}^{(n)}$ terms. Figure 3(a) shows two unstable discontinuities. Figure 3(b) shows a stable and an unstable discontinuity. $\psi_\alpha^{(1)}$ and $\psi_\alpha^{(3)}$ will converge where $\psi_\alpha^{(3)} \approx 0.2$, $\psi_\alpha^{(2)}$ and $\psi_\alpha^{(3)}$ will diverge where $\psi_\alpha^{(3)} \approx 0.6$. Both figures show potential boundedness problems. For example, the positive source terms for $\psi_\alpha^{(3)} > 0.6$ and the negative source term for $\psi_\alpha^{(3)} < 0.2$ in Figure 3(a).

The diffusion terms for $N > 3$ particle systems show more instances of the behaviour illustrated in Figure 3, up to a maximum of $N - 1$ discontinuities.

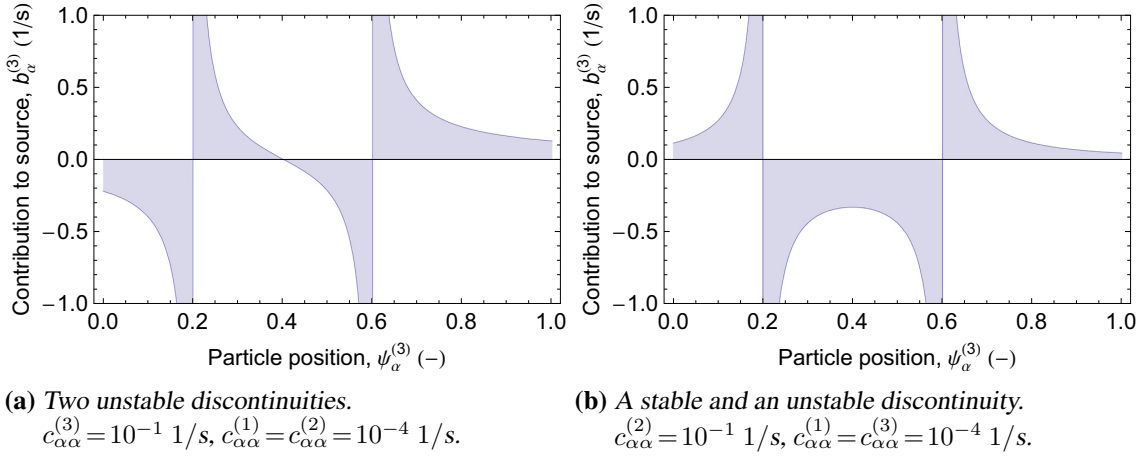


Figure 3: Functional form of the diffusion source term for an $N = 3$ particle system.

The source term is shown as a function of the particle position $\psi_\alpha^{(3)}$ where $\psi_\alpha^{(1)} = 0.2$, $\psi_\alpha^{(2)} = 0.6$ and $w^{(1)} = w^{(2)} = w^{(3)} = 1/3$.

The numerical integration of the diffusion term presents several challenges. At a stable discontinuity, the particles will converge and the discontinuity will persist. The risk is that the solution may ‘overshoot’ and oscillate about the discontinuity. At an unstable discontinuity, the particles will diverge. The sign of the diffusion term will determine the direction of divergence. However, the source term is singular at the discontinuity. The sign is undefined and may not necessarily be arbitrarily assigned. The diffusion term may lead to violations of boundedness. This is most likely in regions of high turbulence and high scalar gradients. Analogous issues arise due to the turbulent diffusion process in other Eulerian particle methods, for example the Stochastic Fields method [8, 9].

3.2.2 General solver

A general DQMoM-IEM solver was developed to numerically integrate equation (23) using RADAU5 [11], an implicit 5th order Runge-Kutta method with low start-up cost. The source terms $b_\alpha^{(n)}$ are supplied by *functional evaluation*. The diffusion term is modified to address the issues highlighted in Figures 2 and 3. Equation (25) is rewritten

$$b_\alpha^{(n)} = w^{(n)} r_\alpha^{(n)} + f_b(\psi_\alpha^{(n)}, b_{dx_\alpha}^{(n)}), \quad (27)$$

where

$$b_{dx_\alpha}^{(n)} = w^{(n)} c_{\alpha\alpha}^{(n)} \sum_{\substack{i=1 \\ i \neq n}}^N f_p(\psi_\alpha^{(n)} - \psi_\alpha^{(i)}) + \prod_{\substack{i=1 \\ i \neq n}}^N f_p(\psi_\alpha^{(n)} - \psi_\alpha^{(i)}) \left[\sum_{\substack{j=1 \\ j \neq n}}^N w^{(j)} c_{\alpha\alpha}^{(j)} \prod_{\substack{k=1 \\ k \neq j, n}}^N (\psi_\alpha^{(j)} - \psi_\alpha^{(k)}) \right], \quad (28)$$

and

$$f_b(\psi, b_{dx}) = \begin{cases} b_{dx} f\left(\frac{ub - \psi}{\varepsilon_b}\right) & \text{if } b_{dx} > 0 \text{ and } ub - \psi > 0 \\ b_{dx} f\left(\frac{\psi - lb}{\varepsilon_b}\right) & \text{if } b_{dx} < 0 \text{ and } \psi - lb > 0 \\ 0 & \text{otherwise,} \end{cases} \quad (29)$$

$$f_p(\Delta\psi) = \begin{cases} \frac{1}{\Delta\psi} f\left(\frac{\Delta\psi}{\varepsilon_p}\right) & \text{if } \Delta\psi \neq 0 \\ 0 & \text{otherwise.} \end{cases} \quad (30)$$

A *bounding function* $f_b(\psi, b_{dx})$ is used to clip the diffusion term to enforce boundedness. The lower bound lb and upper bound ub are defined for each $\psi_\alpha^{(n)}$

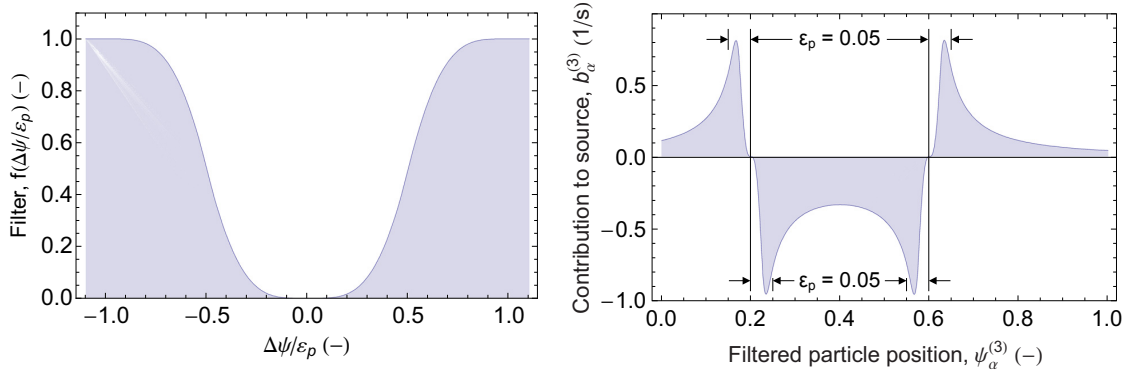
$$lb_\alpha^{(n)} = \max[lb_{gb}, \min(\{\psi_\alpha^{(n)}\}_{nb})] \quad (31)$$

$$ub_\alpha^{(n)} = \min[ub_{gb}, \max(\{\psi_\alpha^{(n)}\}_{nb})] \quad (32)$$

where $\{\cdot\}_{\text{nb}}$ denotes the set of Star-CD neighbour cells and $[lb_{\text{gb}}, ub_{\text{gb}}]$ is a global bound interval imposed over the entire domain. In the case of mass fractions $[lb_{\text{gb}}, ub_{\text{gb}}] = [0, 1]$.

A *particle function* $f_p(\Delta\psi)$ is used to control the discontinuities and singularities. Several approaches were considered. The most obvious is to impose a minimum particle separation. This avoids singularities, but not discontinuities. It risks limiting the effect of the diffusion term and would not necessarily prevent oscillation of the numerical solution about a stable discontinuity. The same reasoning may be applied to approaches that limit the maximum value of the diffusion term or set it to zero near a discontinuity. A less arbitrary approach is to replace the discontinuity and singularity with a smooth transition.

A symmetrical *filter function* $f(\Delta\psi/\varepsilon_p)$ is used by the particle function to remove the discontinuities. The effect of the filter function on the diffusion source term is illustrated in Figure 4. An exaggerated value of ε_p is used for clarity. The diffusion term is set to zero at and slightly to either side of each discontinuity. The zero region negates the requirement to assign an arbitrary sign to the diffusion term. The width of the region can be used to prevent oscillation of the numerical solution without changing the RADAU5 tolerances. The same filter is used by the bounding function to ensure smooth clipping at the bounds. ε_p and ε_b are small positive numbers. In the current implementation $\varepsilon_b = \varepsilon_p = 10^{-3}$.



(a) Filter function.

(b) Filtered source term from Figure 3(b).

Figure 4: Filtered diffusion source term for an $N = 3$ particle system.

The filter function preserves as much of the diffusion term as possible. However, a side-effect is that the diffusion terms on each particle only sum to zero for an $N = 2$ particle system with a symmetric filter. This is also the case where a maximum value is imposed on the diffusion term instead of using a filter. A similar problem is presented where the diffusion term is clipped to enforce boundedness. In general, the diffusion term cannot be modified for one scalar on a given particle without disturbing the scalar mean and mass balance over the set of particles. The diffusion term $f_b(\psi_\alpha^{(n)}, b_{\text{dx}_\alpha}^{(n)})$ calculated using equation (27) is normalised to enforce mass balance and conservation of the scalar mean.

3.2.3 Full analytic solver

An efficient solver was developed to analytically integrate the $N = 2$ particle case for scalars with no chemical source term. Equation (23) is rewritten as

$$\frac{\partial s_\alpha^{(n)}}{\partial t} = \mathcal{F}_{\text{mx}_\alpha}^{(n)} + \mathcal{F}_{\text{dx}_\alpha}^{(n)}, \quad (33)$$

and integrated using an additional second-order operator splitting

$$\text{Step i:} \quad s_\alpha^{(n)\dagger 1} = s_\alpha^{(n)}(t) + \int_0^{\frac{1}{2}\Delta t} \mathcal{F}_{\text{mx}_\alpha}^{(n)} d\tau \quad \text{with } s_\alpha^{(n)} = s_\alpha^{(n)}(t) \text{ at } \tau = 0, \quad (34)$$

$$\text{Step ii:} \quad s_\alpha^{(n)\dagger 2} = s_\alpha^{(n)\dagger 1} + \int_0^{\Delta t} \mathcal{F}_{\text{dx}_\alpha}^{(n)} d\tau \quad \text{with } s_\alpha^{(n)} = s_\alpha^{(n)\dagger 1} \text{ at } \tau = 0, \quad (35)$$

$$\text{Step iii:} \quad s_\alpha^{(n)}(t + \Delta t) = s_\alpha^{(n)\dagger 2} + \int_0^{\frac{1}{2}\Delta t} \mathcal{F}_{\text{mx}_\alpha}^{(n)} d\tau \quad \text{with } s_\alpha^{(n)} = s_\alpha^{(n)\dagger 2} \text{ at } \tau = 0. \quad (36)$$

The operators are defined

$$\mathcal{F}_{\text{mx}_\alpha}^{(n)} = w^{(n)} \frac{C_\phi}{2\tau_\phi} (\langle \phi_\alpha \rangle_N - \psi_\alpha^{(n)}) \quad n \in \{1, 2\}, \quad (37)$$

$$\mathcal{F}_{\text{dx}_\alpha}^{(n)} = \frac{w^{(1)} c_{\alpha\alpha}^{(1)} + w^{(2)} c_{\alpha\alpha}^{(2)}}{\psi_\alpha^{(n)} - \psi_\alpha^{(i)}} \quad n, i \in \{1, 2\}, i \neq n, \quad (38)$$

and are integrated analytically

$$\int_{t_1}^{t_2} \mathcal{F}_{\text{mx}_\alpha}^{(n)} d\tau = w^{(1)} w^{(2)} \Delta\psi_\alpha^{(n)} \left(1 - \exp \left[-\frac{C_\phi}{2\tau_\phi} (t_2 - t_1) \right] \right) \quad (39)$$

$$\int_{t_1}^{t_2} \mathcal{F}_{\text{dx}_\alpha}^{(n)} d\tau = w^{(1)} w^{(2)} \Delta\psi_\alpha^{(n)} \pm \sqrt{2(t_2 - t_1) w^{(1)} w^{(2)} \left(w^{(1)} c_{\alpha\alpha}^{(1)} + w^{(2)} c_{\alpha\alpha}^{(2)} \right) + \left(w^{(1)} w^{(2)} \Delta\psi_\alpha^{(n)} \right)^2}, \quad (40)$$

where

$$\Delta\psi_\alpha^{(n)} = \psi_\alpha^{(i)}(t_1) - \psi_\alpha^{(n)}(t_1) \quad n, i \in \{1, 2\}, i \neq n.$$

The values of the micromixing parameters C_ϕ and τ_ϕ , weights $w^{(n)}$ and terms in $c_{\alpha\alpha}^{(n)}$ are treated as constant during the integration as per Section 3.1.

The root in equation (40) is chosen so that the particles diverge as per the behaviour illustrated in Figure 2. If $\Delta\psi_\alpha^{(n)} < 0$, the positive root is chosen. If $\Delta\psi_\alpha^{(n)} > 0$, the negative root is chosen. If $\Delta\psi_\alpha^{(n)} = 0$, the right hand side of equation (40) is set to zero. The current code enforces the mass fraction bounds $[0, 1]$ over the whole domain by clipping the magnitude of the root. No neighbour cells are considered.

The advantage of this solver is that it is very fast. It is general in the sense that it may be applied to any number of scalars, although it is restricted to $N = 2$ particles.

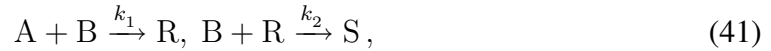
4 Numerical experiments and validation

This section presents the numerical validation of the DQMoM-IEM solvers described in Section 3 against a constant density test case known from the literature.

Section 4.1 describes salient details of the test case. Section 4.2 describes the validation of the solvers against the method of moments. This validates the treatment of the diffusion term described in Section 3. Section 4.3 demonstrates the application of the general solver to a reacting test case. Sections 4.4 and 4.5 discuss the solver efficiency in terms of CPU time and the significance of the choice of boundary conditions.

4.1 Model problem

The investigations in this paper were performed using a constant density test case known from the literature. This was selected because it has been well studied numerically [23, 24] and experimentally [14]. The system considered is the isothermal liquid-phase reaction:



where $k_1 = 5.0 \times 10^6 \text{ m}^3/\text{kmol s}$ and $k_2 = 1.8 \times 10^3 \text{ m}^3/\text{kmol s}$ [23]. In regions where mixing is slow relative to the second reaction, a significant proportion of B and R react to form S before B can be quenched by further mixing with A. The yield of R defined by

$$Y = \frac{C_R}{C_R + 2C_S}, \quad (42)$$

is sensitive to the rate of mixing. The case offers a simple approximation to stiff chemistry.

The reactor configuration is illustrated in Figure 5. It is the single-jet system studied by Li and Toor [14] and Tsai and Fox [23]. This paper considers the case where a turbulent jet of reactant B is injected into an annular laminar coflow of reactant A. Cases are considered for two jet Reynolds numbers, $Re=3530$ and $Re=7552$, and two inlet concentrations.

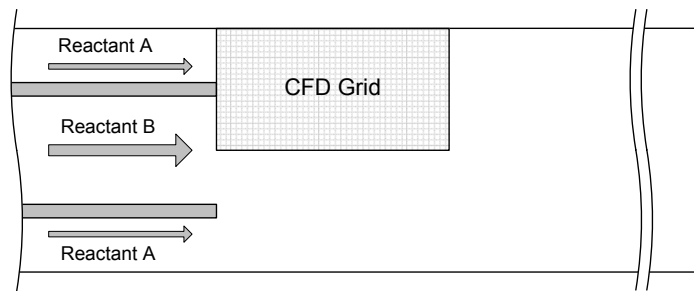


Figure 5: Configuration of the single-jet tubular reactor.

The reactor is modelled in 3D using a triangular prism-shaped domain and boundary conditions to exploit axial symmetry. The flow in the reactor was solved as a steady problem using Star-CD [2] as per the approach detailed by Tsai and Fox [23]. The RANS equations were solved using a $k-\varepsilon$ High Reynolds Number turbulence model and a standard

wall function. The default model constants were used with unit Prandtl numbers. The inlet boundary conditions are summarised in Table 1.

A *base* grid was defined for each Reynolds number using the axial and radial coordinates specified by Tsai and Fox [23, Table 1 and Table 2]. A *refined* grid was defined for each case by dividing each cell in the base grid by a factor of two in the axial direction, and each cell except those adjacent to the outer wall by a factor of two in the radial direction. The exception was made necessary by the wall function, which required the coarse radial resolution at the wall to be retained. All the grids were one cell deep in the circumferential direction. The base grid turbulent kinetic energy k and turbulent dissipation ε fields are presented for the $Re=3530$ and $Re=7552$ cases. See Figures 6 and 7.

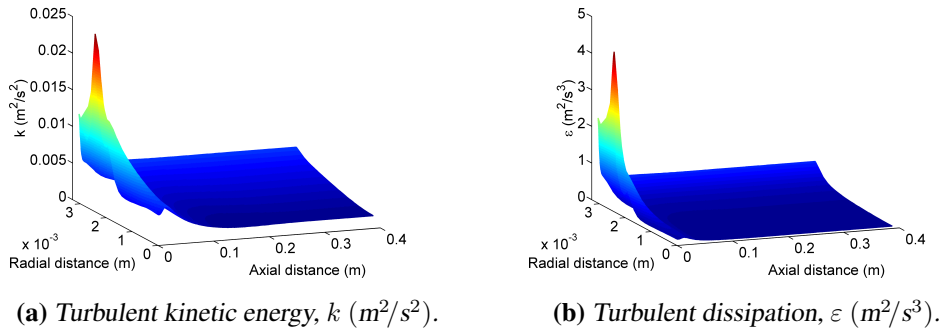


Figure 6: Jet reactor flow field for the base grid at $Re=3530$.

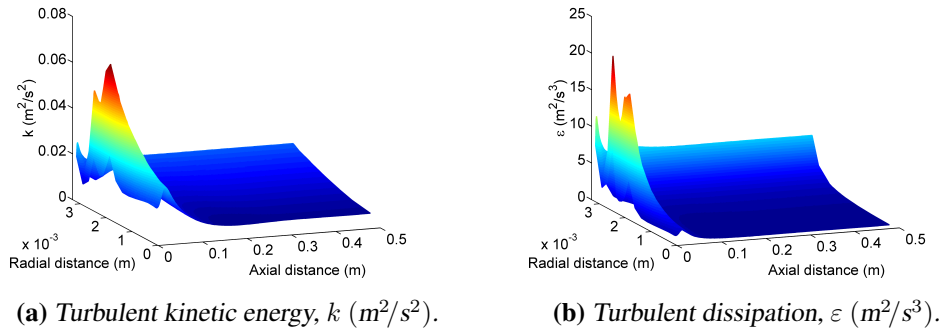


Figure 7: Jet reactor flow field for the base grid at $Re=7552$.

The refined grid data show a modest grid-sensitivity in the peak values of k , ε and ν_T at the inlets. However, the flow fields are considered to be grid-independent *for engineering purposes* based on the grid causing an observed variation of less than 0.2% in the yield of the reacting flow cases presented in Section 4.3.

The DQMoM-IEM scalar transport equations are solved as unsteady problems (see Section 3.1) in Sections 4.2 and 4.3, using the steady flow solutions without re-solving the flow. This one-way coupling is acceptable for the constant density test case. The flow affects the scalars, but the scalars are *passive* and do not affect the flow.

The DQMoM-IEM data are presented in terms of the empirical mean and standard deviation of each species. The composition space is defined in terms of the mass fractions

$$\phi^\top = [Y_A, Y_B, Y_R, Y_S] . \quad (43)$$

The chemical source terms are given by

$$S_\alpha(Y) = S_\alpha(C) \frac{W_\alpha}{C_T} , \quad (44)$$

where the total mass concentration C_T is transported as an additional conserved scalar and

$$\begin{aligned} S_A(C) &= -k_1 C_A C_B \\ S_B(C) &= -k_1 C_A C_B - k_2 C_B C_R \\ S_R(C) &= +k_1 C_A C_B - k_2 C_B C_R \\ S_S(C) &= +k_2 C_B C_R , \end{aligned} \quad (45)$$

$$C_\alpha = \frac{C_T Y_\alpha}{W_\alpha} . \quad (46)$$

Table 1 gives the mass concentration boundary conditions. Mass balance was not used to reduce the number of transport equations. This was a deliberate decision motivated by a desire to keep the test case general. Likewise, the option to use a mixture fraction approach is acknowledged, but was not pursued.

The micromixing parameters are given as $C_\phi = 1.65$ and $\tau_\phi = d/\sqrt{k}$, where $d = 0.0066$ m is the diameter of the reactor [23]. The turbulent diffusivity Γ_T is calculated $\Gamma_T = \nu_T/\sigma_T$, where the turbulent Schmidt number is given $\sigma_T = 0.7$ for all scalars [24]. The turbulent kinetic energy k and turbulent viscosity ν_T are supplied by Star-CD.

Table 1: Model problem: Inlet boundary conditions.

| | | Re=3530 case | | Re=7552 case | |
|-----------------------|----------------------|-----------------------------|---------------------------------|-----------------------------|---------------------------------|
| | | Jet | Annulus | Jet | Annulus |
| Volumetric flow | (m ³ /s) | 0.988 × 10 ⁻⁵ | | 2.11 × 10 ⁻⁵ | |
| Average velocity | (m/s) | 0.786 | 0.613 | 1.68 | 1.13 |
| Mixing length | (m) | 28 × 10 ⁻⁵ | 6.3 × 10 ⁻⁵ | 28 × 10 ⁻⁵ | 6.3 × 10 ⁻⁵ |
| Turbulence intensity | (%) | 5.76 | 4.00 | 5.24 | 4.00 |
| Density | (kg/m ³) | 998 | | | |
| Molecular viscosity | (kg/m s) | 0.889 | | | |
| Mol. wt. (kg/kmol) | | High conc. case | | Low conc. case | |
| | | Jet (kg/m ³) | Annulus (kg/m ³) | Jet (kg/m ³) | Annulus (kg/m ³) |
| Species A | 143.1 | — | 0.426 | — | 0.144 |
| Species B | 183.2 | 0.524 | — | 0.177 | — |

4.2 Solver validation

This section describes the validation of the DQMoM-IEM solvers presented in Section 3. A scalar mixing case is used to validate the treatment of the DQMoM-IEM diffusion term against the method of moments. The application of the method of moments to transported PDF problems is well established and provides an exact solution to equation (1) in the inert case where the chemical source term is null, $S_\alpha = 0$. For readers who would appreciate more detail, the method of moments implementation is summarised in Appendix B.

The scalar mixing of species A and B was investigated for the high concentration case at $Re = 3530$. The empirical mean and standard deviation calculated by DQMoM-IEM with $N = 2$ particles are presented for species A in Figure 8. The mean of species B is given by the complement of Figure 8(a), the standard deviation of species B is identical to Figure 8(b). The boundary and initial conditions are given in Table 5 (see Section 4.5).

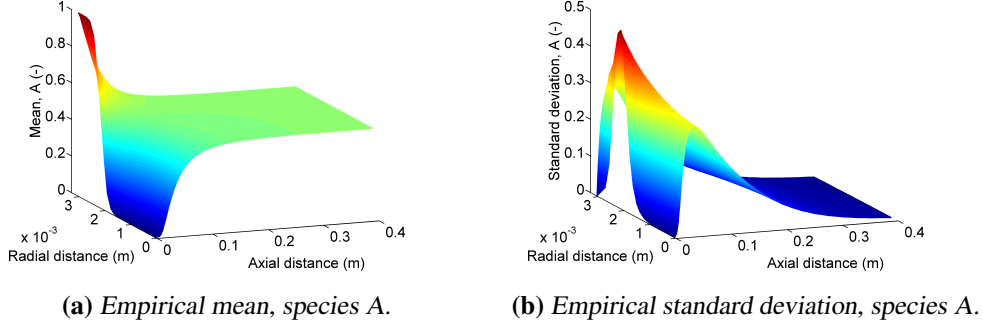


Figure 8: Jet reactor species fields for the inert high concentration case at $Re = 3530$. The case was run on the base grid with time step $\Delta t = 10^{-4}$ s for $t = 2$ s physical time.

The agreement between the DQMoM-IEM solvers was assessed for the first four integer moments and the standard deviation

$$\varepsilon_{m_\alpha} = \frac{1}{N_{\text{cells}}} \sum_{\alpha=1}^K \left\| \left\langle \phi_\alpha^{m_\alpha} \right\rangle_N \Big|_{\text{general solver}} - \left\langle \phi_\alpha^{m_\alpha} \right\rangle_N \Big|_{\text{full analytic solver}} \right\| \quad m_\alpha \in \{1, 2, 3, 4\}, \quad (47)$$

$$\varepsilon_{\text{sd}} = \frac{1}{N_{\text{cells}}} \sum_{\alpha=1}^K \left\| \sqrt{\left\langle \phi_\alpha^2 \right\rangle_N - \left\langle \phi_\alpha \right\rangle_N^2} \Big|_{\text{general solver}} - \sqrt{\left\langle \phi_\alpha^2 \right\rangle_N - \left\langle \phi_\alpha \right\rangle_N^2} \Big|_{\text{full analytic solver}} \right\|, \quad (48)$$

where the norm notation denotes an L^2 -norm over space. The agreement with the method of moments was assessed likewise.

Table 2 shows that the DQMoM-IEM solvers reproduce the method of moments case for the first four integer moments, and give almost identical results for $N = 2$ particles. The $N = 3$ case shows less satisfactory agreement with the method of moments. The differences occur in the region of high spatial gradient between the inlets of species A and B. The differences are attributed to the numerical treatment of the diffusion term, where, in particular, the filtered terms no longer necessarily sum to zero for $N > 2$ (see Section 3.2.2). To the naked eye, all the cases were indistinguishable from Figure 8.

Table 2: DQMoM-IEM validation data for the jet reactor inert high conc. case at $Re=3530$.
The cases were run on the base grid with time step $\Delta t = 10^{-4}$ s for $t = 2$ s physical time.
Case 1: DQMoM-IEM general solver, $N=2$ vs. analytic solver.
Case 2: DQMoM-IEM general solver, $N=2$ vs. method of moments.
Case 3: DQMoM-IEM general solver, $N=3$ vs. method of moments.

| | Integer moments | | | | Standard deviation |
|--------|----------------------------|----------------------------|----------------------------|----------------------------|-----------------------|
| | $\varepsilon_{m_\alpha=1}$ | $\varepsilon_{m_\alpha=2}$ | $\varepsilon_{m_\alpha=3}$ | $\varepsilon_{m_\alpha=4}$ | ε_{sd} |
| Case 1 | 6.98×10^{-9} | 7.55×10^{-8} | 1.13×10^{-7} | 1.43×10^{-7} | 3.37×10^{-7} |
| Case 2 | 3.30×10^{-6} | 1.78×10^{-5} | 3.79×10^{-5} | 7.15×10^{-5} | 4.03×10^{-5} |
| Case 3 | 3.32×10^{-4} | 3.34×10^{-4} | 2.99×10^{-4} | 2.69×10^{-4} | 1.71×10^{-4} |

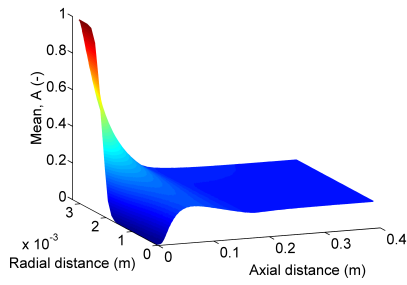
4.3 Solver application to reacting flow

This section describes the application of the DQMoM-IEM general solver presented in Section 3 to a real turbulent reaction chemical engineering problem (see Section 4.1). The results are validated against previous studies of the same system [14, 23].

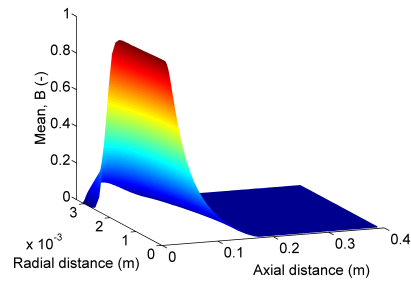
The empirical mean and standard deviations calculated by DQMoM-IEM with $N = 2$ particles are presented in Figures 9 and 10 for the high concentration case at $Re = 3530$. The boundary and initial conditions are summarised in Tables 1 and 5 (see Section 4.5). They are visually consistent with the transported PDF data of Tsai and Fox [23, Fig. 7 and 8 (with the caveat that the scaling makes the standard deviation look less ‘peaky’)].

Figure 9 shows rapid reaction between species A and B, with a small region of coexistence near the wall between the inlets. The product R forms very rapidly in the reaction zone. The side-product S forms more slowly, with most forming in the zone of high concentration of B and R at the centre of the reactor near the jet inlet.

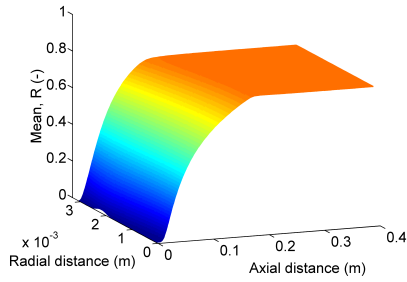
Figure 10(c) shows an arc of zero standard deviation running clockwise from the wall between the inlets to the centre of the reactor at an axial distance of about 0.1 m. This is an artefact of the $N = 2$ particle case. It is caused by the transition from a region where $\psi_R^{(1)} > \psi_R^{(2)}$ near the jet inlet to a region where $\psi_R^{(1)} < \psi_R^{(2)}$ in the bulk of the reactor. The zero standard deviation marks the locus $\psi_R^{(1)} = \psi_R^{(2)}$. In the $N = 3$ particle case, the zero standard deviation does not occur. Rather, there is a shallow local minimum.



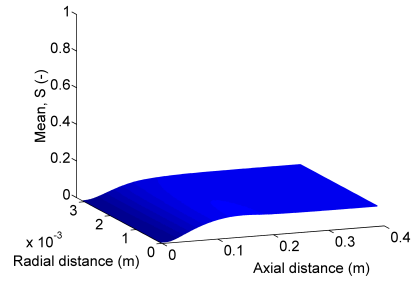
(a) Empirical mean, species A.



(b) Empirical mean, species B.

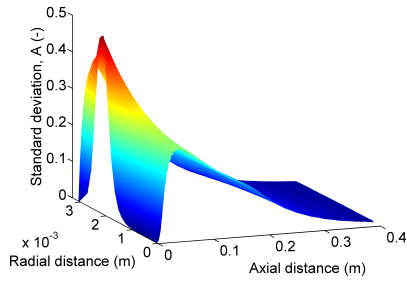


(c) Empirical mean, species R.

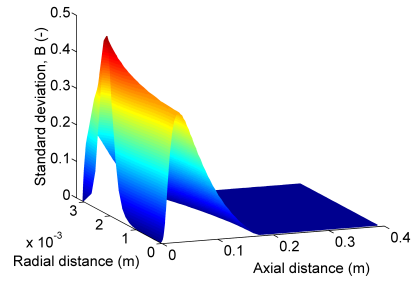


(d) Empirical mean, species S.

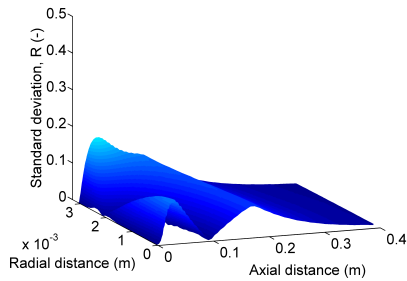
Figure 9: Jet reactor species means for the high concentration case at $Re=3530$.
The case was run on the base grid with time step $\Delta t=10^{-4}$ s for $t=2$ s physical time.



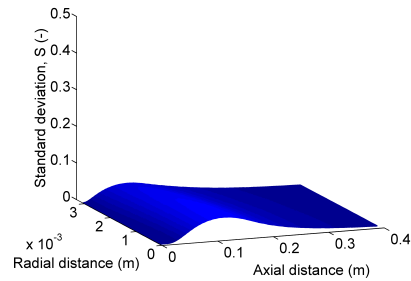
(a) Empirical standard deviation, species A.



(b) Empirical standard deviation, species B.



(c) Empirical standard deviation, species R.



(d) Empirical standard deviation, species S.

Figure 10: Jet reactor species standard deviations for the high concentration case at $Re=3530$.
The case was run on the base grid with time step $\Delta t=10^{-4}$ s for $t=2$ s physical time.

Table 3 summarises the yield for all cases considered. The yields were calculated as per equation (42) and show a grid-sensitivity of less than 0.2%. The solutions are considered to be grid-independent. The $Re = 3530$ high concentration case shows no significant difference for $N = 2, 3$ particles. DQMoM-IEM correctly predicts the effect of the Reynolds number and reactant concentration, but slightly over estimates the yields compared to Tsai and Fox [23] and Li and Toor [14]. Whether this is acceptable will be case specific.

Table 3: DQMoM-IEM reaction yields.

The base grid cases were run with time step $\Delta t = 10^{-4}$ s for $t = 2$ s physical time.

The refined grid cases were run with time step $\Delta t = 4 \times 10^{-5}$ s for $t = 1$ s physical time.

| Case | | DQMoM-IEM yield (%) | | | Transported | Experimental [‡] |
|------|------|---------------------|--------------|-----------|------------------------|---------------------------|
| Conc | Re | $N=2$ | $N=2$ | $N=3$ | PDF yield [†] | yield |
| | | base grid | refined grid | base grid | (%) | (%) |
| High | 3530 | 85.05 | 84.96 | 85.21 | 81.0 | 82.05 |
| High | 7552 | 91.10 | 90.91 | — | 88.3 | 88.33 |
| Low | 3530 | 93.84 | 93.79 | — | 91.8 | 88.95 |
| Low | 7552 | 96.58 | 96.51 | — | 95.4 | 93.45 |

[†] Tsai and Fox [23, Table 3], [‡] Li and Toor [14, Table 1].

4.4 Solver efficiency

Table 4 shows the CPU times for the $Re = 3530$ high concentration cases. The analytic solver showed a significant speed advantage over the general solver with $N = 2$ particles.

The general solver CPU times are comparable between the inert and reacting cases. The inclusion of the test reaction reduces the CPU time in the $N = 3$ case. This is repeatable. It is attributed to the reaction causing the particles to move away from each other in composition space, reducing the impact of the numerical issues that characterise the diffusion term as per Figure 3.

The efficient treatment of the diffusion term represents an important area of future research to make the general solver more practical. One route may be to improve efficiency at the expense of detail where particles approach each other in composition space.

Table 4: DQMoM-IEM CPU times for the jet reactor high concentration case at $Re = 3530$.

The cases were run on the base grid with time step $\Delta t = 10^{-4}$ s for $t = 2$ s physical time.

| | CPU time (s) | |
|-----------------------------------|--------------|---------------|
| | Inert flow | Reacting flow |
| DQMoM-IEM analytic solver | 323 | — |
| DQMoM-IEM general solver, $N = 2$ | 9048 | 9236 |
| DQMoM-IEM general solver, $N = 3$ | 15222 | 12977 |

4.5 Significance of the choice of boundary conditions

The choice of boundary conditions to represent a given physical condition is not arbitrary. Different representations of the *same physical condition* may give different results.

The code development was performed using the inert case and equi-weighted particles such that the observed central moments were solely due to the diffusion term. However, equal weights are a poor choice. For example, an equi-weighted $N = 2$ particle system cannot reproduce Figure 8. The peak standard deviation is significantly restricted by the physical bounds. The correct scalar mixing was only achieved when the boundary conditions were specified to be consistent with each particle being assigned to a specific inlet.

Table 5 summarises the boundary and initial conditions for Figures 8-10 and Tables 2-4. The $N = 2$ case is specified such that particle 1 represents the annular inlet and particle 2 the jet inlet. The $N = 3$ case is specified such that particle 1 represents the annular inlet and particles 2 and 3 represent the jet inlet. The rationale for the extra particle at the jet is that it gave slightly better agreement with the method of moments. The initial conditions were specified to be consistent with the inlet boundaries whilst avoiding equal $\psi_\alpha^{(n)}$.

Table 5: DQMoM-IEM inlet boundary and initial conditions.

The positions are specified in terms of $\psi_\alpha^{(n)}$ for clarity. The transported variables are the weights $w^{(n)}$ and weighted positions $s_\alpha^{(n)} = w^{(n)}\psi_\alpha^{(n)}$.

| | $N = 2$ case | | | $N = 3$ case | | |
|--------------------|----------------|---------|--------------------|----------------|---------|--------------------|
| | Inlet boundary | | Initial condition | Inlet boundary | | Initial condition |
| | Jet | Annulus | | Jet | Annulus | |
| $w^{(1)}$ | 0 | 1 | 1/2 | 0 | 1 | 1/3 |
| $w^{(2)}$ | 1 | 0 | 1/2 | 1/2 | 0 | 1/3 |
| $w^{(3)}$ | — | — | — | 1/2 | 0 | 1/3 |
| $\psi_A^{(1)}$ | 0 | 1 | 1 | 0 | 1 | 1 |
| $\psi_A^{(2)}$ | 0 | 1 | 0 | 0 | 1 | 1/2 |
| $\psi_A^{(3)}$ | — | — | — | 0 | 1 | 0 |
| $\psi_B^{(n)}$ | 1 | 0 | $1 - \psi_A^{(n)}$ | 1 | 0 | $1 - \psi_A^{(n)}$ |
| $\psi_{R,S}^{(n)}$ | 0 | 0 | 0 | 0 | 0 | 0 |

This specification of boundary conditions is perhaps intuitive considering the evolution of DQMoM-IEM from multi-environment presumed PDF methods [5]. DQMoM-IEM should be interpreted as an environment model. The number of inlets should dictate the *minimum* number of particles. The benefit of extra particles is illustrated by the change in the region of zero standard deviation between the $N = 2$ and $N = 3$ particle reacting flow cases, see Figure 10(c).

5 Conclusions

The numerical behaviour of DQMoM-IEM has been investigated as a turbulent reaction closure. DQMoM-IEM uses a deterministic particle method to approximate the joint composition PDF. It is attractive because it may offer a computationally efficient turbulent reaction method suitable for engineering calculations using standard software.

An *analytic expression* has been derived for the DQMoM-IEM source terms. It is valid for any number of particles and scalars. Explicit *reaction*, *micromixing* and turbulent *diffusion* terms can be identified. The diffusion term may cause loss of boundedness. It is discontinuous and singular if two or more particle positions are equal in *any* dimension of composition space.

Two DQMoM-IEM solvers have been coupled to the Star-CD CFD code using an operator splitting method. They have been validated against the method of moments and a reacting flow case. The choice of boundary conditions to represent a given physical condition is not arbitrary. The correct scalar mixing was only reproduced when the boundary conditions were specified to be consistent with each particle being assigned to a specific inlet.

The first (general) solver can be applied to cases with any number of particles and scalars. The diffusion terms are calculated by *functional evaluation* and are filtered to eliminate discontinuities and enforce boundedness. The approach is similar to methods that limit the size of the diffusion term or set it to zero near a discontinuity. It differs in that it preserves more information and eliminates the discontinuity, which the other methods would not. The source terms are integrated numerically using the RADAU5 implicit ODE solver.

The second (analytic) solver is specific to $N = 2$ particles. It uses *analytic solutions* of the DQMoM-IEM terms arising due to turbulent diffusion and micromixing and may be applied to any number of scalars.

The key challenge in the methodology is the *efficient* integration of the diffusion terms. The analytic solver provides an elegant approach to the $N = 2$ particle case. The numerical treatment of the diffusion term by the general solver was considered in detail and demonstrated for $N = 2$ and $N = 3$ particles, and remains an important area of future research to make the method more practical.

Acknowledgements

The authors thank reSolutions Ltd. and the EPSRC (grant EP/C537564/1) for the financial support of Jethro Akroyd, and Dr Simon Lo of CD-adapco for licences and technical support of Star-CD.

The authors gratefully thank Christopher Handscomb and Sebastian Mosbach for their time and advice.

Nomenclature

Upper-case Roman

| | |
|--------------------|---|
| A | DQMoM coefficient matrix, see Eq. (A.16) |
| A_1 | DQMoM coefficient matrix, see Eqs. (A.16) and (A.23) |
| A_2 | DQMoM coefficient matrix, see Eqs. (A.16), (A.21) and (A.24) |
| A_3 | DQMoM coefficient matrix, see Eqs. (A.16), (A.22) and (A.25) |
| \mathcal{C}_T | Total mass concentration |
| C_α | Molar concentration of species α |
| C_ϕ | IEM micromixing model constant |
| \mathcal{F}_1 | DQMoM-IEM source term operator, see Eqs. (14), (18) and (19) |
| \mathcal{F}_2 | DQMoM-IEM physical space advection and diffusion operator, see Eqs. (14), (20) and (21) |
| \mathcal{F}_{dx} | DQMoM-IEM diffusion term operator, see Eqs. (33) and (38) |
| \mathcal{F}_{mx} | DQMoM-IEM micromixing term operator, see Eqs. (33) and (37) |
| K | Number of scalars |
| M | Number of moments |
| N | Number of particles |
| N_{cells} | Number of cells in the CFD domain |
| $R_\lambda(x, t)$ | Micromixing and chemical source term for λ , see Eq. (B.1) |
| Re | Reynolds number |
| $S(\phi)$ | Chemical source term vector |
| $U(x, t)$ | Eulerian velocity vector |
| W_2 | Diagonal matrix of the particle weights $w^{(n)}$, see Eq. (A.26) |
| W_3 | Diagonal matrix of the particle weights $w^{(n)}$, see Eq. (A.27) |
| W_α | Relative molecular mass of scalar α |
| Y | Yield of the test reaction, see Eq. (42) |
| Y_α | Mass fraction of scalar α |

Lower-case Roman

| | |
|-------------------------------|---|
| $a^{(n)}$ | Source term for the weights $w^{(n)}$, see Eq. (5) |
| $b_\alpha^{(n)}$ | Source term for the weighted positions $s_\alpha^{(n)}$, see Eq. (6) |
| $c_{\alpha\beta}^{(n)}$ | Turbulent diffusion-spatial gradient term, see Eq. (12) |
| d | Diameter scale in IEM micromixing model, $\tau_\phi = d/\sqrt{k}$ |
| $f(\Delta\psi/\varepsilon_p)$ | Filter function, see Eq. (30) |
| $f_b(\psi, b_{dx})$ | Bounding function, see Eq. (29) |
| $f_p(\Delta\psi)$ | Particle function, see Eq. (30) |
| $f_\phi(\psi; x, t)$ | Joint composition PDF of the random scalar field $\phi(x, t)$ |

| | |
|------------------|--|
| k | Turbulent kinetic energy |
| k_1 | Reaction rate constant for the test reaction, see Eq. (41) |
| k_2 | Reaction rate constant for the test reaction, see Eq. (41) |
| lb | Lower bound, see Eq. (29) |
| m_α | Moment order of scalar α |
| $m_{m\alpha}$ | Moment order of scalar α in the m^{th} empirical moment $\langle \phi_1^{m_{m1}} \dots \phi_K^{m_{mK}} \rangle_N$ of the DQMoM particle system, see Eq. (8) |
| $r_\alpha^{(n)}$ | Micromixing and chemical source term, see Eq. (13) |
| $s_\alpha^{(n)}$ | Weighted particle position, see Eq. (7) |
| t | Time |
| $u(x, t)$ | Fluctuating velocity field $u = U - \langle U \rangle$ |
| ub | Upper bound, see Eq. (29) |
| $w^{(n)}$ | Weight of particle n , see Eq. (2) |
| x | Position vector |

Upper-case Greek

| | |
|-----------------|--|
| Γ_T | Turbulent diffusivity |
| Γ_α | Thermal diffusivity of scalar α |

Lower-case Greek

| | |
|------------------------------------|---|
| α | Vector of DQMoM source terms a and b_α , see Eq. (A.17) |
| β | Vector of DQMoM terms, see Eq. (A.18) |
| $\delta_{\psi_\alpha^{(n)};x,t}$ | Dirac delta function, see Eq. (3) |
| $\delta'_{\psi_\alpha^{(n)};x,t}$ | First derivative of $\delta_{\psi_\alpha^{(n)};x,t}$ with respect to ψ_α |
| $\delta''_{\psi_\alpha^{(n)};x,t}$ | Second derivative of $\delta_{\psi_\alpha^{(n)};x,t}$ with respect to ψ_α |
| ε | Turbulent dissipation rate |
| ε_b | Bounding function clipping distance, see Eq. (29) |
| ε_{m_α} | Error metric for the empirical moment $\langle \phi_\alpha^{m_\alpha} \rangle_N$, see Eq. (47) |
| ε_p | Particle function filter half-width, see Eq. (30) |
| ε_{sd} | Error metric for the empirical standard deviation, see Eq. (48) |
| λ | Moment of the joint composition PDF f_ϕ , see Eq. (B.1) |
| ν_T | Turbulent viscosity |
| σ_T | Turbulent Schmidt number |
| τ_ϕ | IEM micromixing model mixing time |
| $\phi(x, t)$ | Eulerian passive scalar (composition) vector |
| ψ | Sample space variable corresponding to ϕ |
| $\psi_\alpha^{(n)}$ | Position of particle n , see Eq. (2) |

Superscripts

(n) Denotes the n^{th} particle

Subscripts

dx Denotes the diffusion term

gb Denotes a global bound

i Denotes the i^{th} direction

m Denotes the m^{th} moment

mx Denotes the micromixing term

n Denotes the n^{th} particle

nb Denotes a neighbour cell

α Denotes the α^{th} scalar

β Denotes the β^{th} scalar

γ Denotes the γ^{th} scalar

Symbols

\top Transpose operator

∇ Gradient operator

∇^2 Laplacian operator

$\langle \cdot \rangle$ Expectation

$\langle \cdot | \psi \rangle$ Expectation conditioned on $\phi = \psi$

$\langle \cdot \rangle_N$ Empirical expectation over N particles

$\langle \phi_\alpha \rangle_N$ Empirical mean of ϕ_α over N particles

$\langle \phi_\alpha^2 \rangle_N$ Empirical second moment of ϕ_α over N particles

Abbreviations

AMG Algebraic multigrid

CPU Central processing unit

CFD Computational fluid dynamics

DQMOM Direct quadrature method of moments

IEM Interaction by exchange with the mean

LES Large-eddy simulation

MoMIC Method of moments with interpolative closure

ODE Ordinary differential equation

PBE Population balance equation

PDF Probability density function

QMoM Quadrature method of moments

RANS Reynolds-averaged Navier-Stokes

SF Stochastic Fields method

References

- [1] S. R. Cant and E. Mastorakos. *An Introduction to Turbulent Reacting Flows*. Imperial College Press, 2008.
- [2] CD-adapco. Star-CD v4.02.002. URL <http://www.cd-adapco.com/>.
- [3] R. Fan and R. O. Fox. Segregation in polydisperse fluidized beds: Validation of a multi-fluid model. *Chemical Engineering Science*, 63(1):272–285, 2008. doi:10.1016/j.ces.2007.09.038.
- [4] R. Fan, D. L. Marchisio, and R. O. Fox. Application of the direct quadrature method of moments to polydisperse gas-solid fluidized beds. *Powder Technology*, 139(1): 7–20, 2004. doi:10.1016/j.powtec.2003.10.005.
- [5] R. O. Fox. *Computational Models for Turbulent Reacting Flows*. Cambridge University Press, Cambridge, 2003.
- [6] M. Frenklach. Method of moments with interpolative closure. *Chemical Engineering Science*, 57(12):2229–2239, 2002. doi:10.1016/S0009-2509(02)00113-6.
- [7] M. Frenklach and S. J. Harris. Aerosol dynamics modeling using the method of moments. *Journal of Colloid and Interface Science*, 118(1):252–261, 1987. doi:10.1016/0021-9797(87)90454-1.
- [8] A. Garmory. *Micromixing Effects in Atmospheric Reacting Flows*. PhD thesis, University of Cambridge, 2007.
- [9] A. Garmory, E. S. Richardson, and E. Mastorakos. Micromixing effects in a reacting plume by the Stochastic Fields method. *Atmospheric Environment*, 40(6):1078–1091, 2006. doi:10.1016/j.atmosenv.2005.11.002.
- [10] A. Garmory, I. S. Kim, R. E. Britter, and E. Mastorakos. Simulations of the dispersion of reactive pollutants in a street canyon, considering different chemical mechanisms and micromixing. *Atmospheric Environment*, pages 1–11, 2008. doi:10.1016/j.atmosenv.2008.07.033.
- [11] E. Hairer and G. Wanner. *Solving Ordinary Differential Equations II. Stiff and Differential-Algebraic Problems*, volume 14 of *Springer Series in Computational Mathematics*. Springer Verlag, Berlin, second revised edition, 1996.
- [12] W. P. Jones and S. Navarro-Martinez. Large eddy simulation of autoignition with a subgrid probability density function method. *Combustion and Flame*, 150(3):170–187, 2007. doi:10.1016/j.combustflame.2007.04.003.
- [13] W. P. Jones, S. Navarro-Martinez, and O. Röhl. Large eddy simulation of hydrogen auto-ignition with a probability density function method. *Proceedings of the Combustion Institute*, 31(2):1765–1771, 2007. doi:10.1016/j.proci.2006.07.041.

- [14] K. T. Li and H. L. Toor. Turbulent reactive mixing with a series-parallel reaction: Effect of mixing on yield. *AIChE Journal*, 32(8):1312–1320, 1986. doi:10.1002/aic.690320809.
- [15] D. L. Marchisio and R. O. Fox. Solution of population balance equations using the direct quadrature method of moments. *Journal of Aerosol Science*, 36(1):43–73, 2005. doi:10.1016/j.jaerosci.2004.07.009.
- [16] R. McGraw. Description of aerosol dynamics by the quadrature method of moments. *Aerosol Science and Technology*, 27(2):255–349, 1997. doi:10.1080/02786829708965471.
- [17] R. Mustata, L. Valiño, C. Jiménez, W. P. Jones, and S. Bondi. A probability density function Eulerian Monte Carlo field method for large eddy simulations: Application to a turbulent piloted methane/air diffusion flame (sandia d). *Combustion and Flame*, 145(1-2):88–104, 2006. doi:10.1016/j.combustflame.2005.12.002.
- [18] S. B. Pope. PDF methods for turbulent reacting flows. *Progress in Energy and Combustion Science*, 11(2):119–192, 1985. doi:10.1016/0360-1285(85)90002-4.
- [19] S. B. Pope. *Turbulent Flows*. Cambridge University Press, Cambridge, 2000.
- [20] V. Raman, H. Pitsch, and R. O. Fox. Eulerian transported probability density function sub-filter model for large-eddy simulations of turbulent combustion. *Combustion Theory and Modelling*, 10(3):439–548, 2006. doi:10.1080/13647830500460474.
- [21] V. Sabel’nikov and O. Souldard. Rapidly decorrelating velocity-field model as a tool for solving one-point Fokker-Planck equations for probability density functions of turbulent reactive scalars. *Physical Review E*, 72(1):Article No. 016301, 2005. doi:10.1103/PhysRevE.72.016301.
- [22] Q. Tang, W. Zhao, M. Bockelie, and R. O. Fox. Multi-environment probability density function method for modelling turbulent combustion using realistic chemical kinetics. *Combustion Theory and Modelling*, 11(6):889–907, 2007. doi:10.1080/13647830701268890.
- [23] K. Tsai and R. O. Fox. PDF simulation of a turbulent series-parallel reaction in an axisymmetric reactor. *Chemical Engineering Science*, 49(24B):5154–5158, 1994. doi:10.1016/0009-2509(94)00270-3.
- [24] K. Tsai, P. A. Gillis, S. Sen, and R. O. Fox. A finite-mode PDF model for turbulent reacting flows. *Journal of Fluids Engineering*, 124(1):102–107, 2002. doi:10.1115/1.1431546.
- [25] L. Valiño. A field Monte Carlo formulation for calculating the probability density function of a single scalar in a turbulent flow. *Flow, Turbulence and Combustion*, 60(2):157–172, 1998. doi:10.1023/A:1009968902446.

- [26] J. Villermaux and J. C. Devillon. Représentation de la coalescence et de la redispersion des domaines de ségrégation dans un fluide par un modèle d'interaction phénoménologique. In *Proceedings of the 2nd International Symposium on Chemical Reaction Engineering*, pages 1–13. International Symposium on Chemical Reaction Engineering, Elsevier, New York, 1972.
- [27] L. Wang and R. O. Fox. Comparison of micromixing models for CFD simulation of nanoparticle formation. *AIChE Journal*, 50(9):2217–2232, 2004. doi:10.1002/aic.10173.
- [28] D. L. Wright, R. McGraw, and D. E. Rosner. Bivariate extension of the quadrature method of moments for modeling simultaneous coagulation and sintering of particle populations. *Journal of Colloid and Interface Science*, 236(2):242–251, 2001. doi:10.1006/jcis.2000.7409.
- [29] A. Zucca, D. L. Marchisio, A. A. Baressi, and R. O. Fox. Implementation of the population balance equation in CFD codes for modelling soot formation in turbulent flames. *Chemical Engineering Science*, 61(1):87–95, 2006. doi:10.1016/j.ces.2004.11.061.
- [30] A. Zucca, D. L. Marchisio, M. Vanni, and A. A. Barresi. Validation of bivariate DQMoM for nanoparticle simulation. *AIChE Journal*, 53(4):918–931, 2007. doi:10.1002/aic.11125.

Citation Index

CD-adapco [2], 4, 7, 14
Cant and Mastorakos [1], 3
Fan and Fox [3], 4
Fan et al. [4], 4
Fox [5], 3, 5, 6, 21
Frenklach and Harris [7], 3
Frenklach [6], 3
Garmory et al. [10], 4
Garmory et al. [9], 11
Garmory [8], 11
Hairer and Wanner [11], 9, 11
Jones and Navarro-Martinez [12], 4
Jones et al. [13], 4
Li and Toor [14], 4, 14, 18, 20
Marchisio and Fox [15], 3
McGraw [16], 3
Mustata et al. [17], 4
Pope [18], 3
Pope [19], 3
Raman et al. [20], 4
Sabel'nikov and Souldard [21], 4
Tang et al. [22], 4
Tsai and Fox [23], 4, 14–16, 18, 20
Tsai et al. [24], 4, 14, 16
Valiño [25], 4
Villermaux and Devillon [26], 3
Wang and Fox [27], 4, 9
Wright et al. [28], 3
Zucca et al. [29], 4
Zucca et al. [30], 4

A DQMoM derivation

The derivations of DQMoM and DQMoM-IEM are well documented in the literature and are described in detail by Fox [5, Appendix B]. This sections summarises the derivations in a general multivariate component form and may be of particular use to anyone who wishes to implement DQMoM.

The text by Fox [5] is recommended to readers who would like more detail.

A.1 DQMoM

The derivation starts with a transport equation for the one-point one-time joint composition PDF f_ϕ [18]. This equation is exact and contains no approximations

$$\frac{\partial f_\phi}{\partial t} + \frac{\partial}{\partial x_i} [f_\phi (\langle U_i \rangle + \langle u_i | \psi \rangle)] = - \frac{\partial}{\partial \psi_\alpha} [f_\phi (\langle \Gamma_\alpha \nabla^2 \phi_\alpha | \psi \rangle + S_\alpha(\psi))] . \quad (\text{A.1})$$

The turbulent convective flux $f_\phi \langle u | \psi \rangle$ and molecular diffusion $\langle \Gamma_\alpha \nabla^2 \phi_\alpha | \psi \rangle$ terms need to be closed. $S_\alpha(\psi)$ is the chemical source term. It describes the material and energy balance of species α and is closed.

Equation (A.1) is closed using a gradient diffusion model for the convective flux, and an IEM model to approximate the molecular diffusion [26]

$$-f_\phi \langle u | \psi \rangle = \Gamma_T \nabla f_\phi , \quad (\text{A.2})$$

$$\langle \Gamma_\alpha \nabla^2 \phi_\alpha | \psi \rangle = \frac{C_\phi}{2\tau_\phi} (\langle \phi_\alpha \rangle - \psi_\alpha) , \quad (\text{A.3})$$

where C_ϕ is an empirical constant and τ_ϕ is the scalar mixing time. Equation (A.3) assumes that all scalars mix at the same rate. The turbulent diffusivity Γ_T is calculated

$$\Gamma_T = \nu_T / \sigma_T , \quad (\text{A.4})$$

where the turbulent viscosity ν_T is prescribed by the turbulence model and the turbulent Schmidt number σ_T is typically close to unity. The closed form of equation (A.1) appears in the main text as equation (1) and is written

$$\frac{\partial f_\phi}{\partial t} + \langle U_i \rangle \frac{\partial f_\phi}{\partial x_i} - \frac{\partial}{\partial x_i} \left(\Gamma_T \frac{\partial f_\phi}{\partial x_i} \right) = - \frac{\partial}{\partial \psi_\alpha} \left[\left(\frac{C_\phi}{2\tau_\phi} (\langle \phi_\alpha \rangle - \psi_\alpha) + S_\alpha(\psi) \right) f_\phi \right] . \quad (\text{A.5})$$

The joint composition PDF f_ϕ in equation (A.5) is approximated using a weighted-particle system (equations 2, 3 and 4 in the main text)

$$\begin{aligned} f_\phi(\psi; x, t) \, \mathbf{d}\psi &= f_\phi(\psi_1, \psi_2, \dots, \psi_K; x, t) \, \mathbf{d}\psi_1 \cdots \mathbf{d}\psi_K \\ &\approx \sum_{n=1}^N w^{(n)}(x, t) \prod_{\alpha=1}^K \delta_{\psi_\alpha^{(n)}; x, t} \, \mathbf{d}\psi_\alpha^{(n)} , \end{aligned} \quad (\text{A.6})$$

where

$$\delta_{\psi_\alpha^{(n)};x,t} \equiv \delta [\psi_\alpha - \psi_\alpha^{(n)}(x,t)] , \quad (\text{A.7})$$

$$\sum_{n=1}^N w^{(n)}(x,t) = 1 . \quad (\text{A.8})$$

The system contains $N(K+1)$ unknowns comprising the weights $w^{(n)}$ and positions $\psi_\alpha^{(n)}$, where $n = 1, \dots, N$ particles and $\alpha = 1, \dots, K$ scalars in the composition vector ϕ .

A non-constant coefficient linear equation (A.10) leading to transport equations for the weights (A.11) and weighted positions (A.12) is derived by substituting the weighted-particle approximation (A.6) into the joint composition PDF transport equation (A.5). Suppressing the dependency of the weighted-particle system on x and t gives

$$\begin{aligned} \frac{\partial}{\partial t} \left[\sum_{n=1}^N w^{(n)} \prod_{\alpha=1}^K \delta_{\psi_\alpha^{(n)}} \right] + \left(\langle U_i \rangle - \Gamma_T \frac{\partial}{\partial x_i} \right) \frac{\partial}{\partial x_i} \left[\sum_{n=1}^N w^{(n)} \prod_{\alpha=1}^K \delta_{\psi_\alpha^{(n)}} \right] \\ = - \frac{\partial}{\partial \psi_\alpha} \left[\left(\frac{C_\phi}{2\tau_\phi} (\langle \phi_\alpha \rangle - \psi_\alpha) + S_\alpha(\psi) \right) f_\phi \right] . \end{aligned} \quad (\text{A.9})$$

Evaluating the derivatives by systematic application of the product rule and collecting terms leads to the linear equation in $a^{(n)}$ and $b_\alpha^{(n)}$

$$\begin{aligned} \sum_{n=1}^N \left[\prod_{\alpha=1}^K \delta_{\psi_\alpha^{(n)}} + \sum_{\alpha=1}^K \psi_\alpha^{(n)} \delta'_{\psi_\alpha^{(n)}} \prod_{\substack{\beta=1 \\ \beta \neq \alpha}}^K \delta_{\psi_\beta^{(n)}} \right] a^{(n)} - \sum_{n=1}^N \sum_{\alpha=1}^K \delta'_{\psi_\alpha^{(n)}} \prod_{\substack{\beta=1 \\ \beta \neq \alpha}}^K \delta_{\psi_\beta^{(n)}} \cdot b_\alpha^{(n)} \\ = \sum_{n=1}^N \left[\sum_{\alpha=1}^K \delta''_{\psi_\alpha^{(n)}} \prod_{\substack{\beta=1 \\ \beta \neq \alpha}}^K \delta_{\psi_\beta^{(n)}} \cdot w^{(n)} c_{\alpha\alpha}^{(n)} + \sum_{\alpha=1}^K \sum_{\substack{\beta=1 \\ \beta \neq \alpha}}^K \delta'_{\psi_\alpha^{(n)}} \delta'_{\psi_\beta^{(n)}} \prod_{\substack{\gamma=1 \\ \gamma \neq \beta}}^K \delta_{\psi_\gamma^{(n)}} \cdot w^{(n)} c_{\alpha\beta}^{(n)} \right] \\ - \frac{\partial}{\partial \psi_\alpha} \left[\left(\frac{C_\phi}{2\tau_\phi} (\langle \phi_\alpha \rangle - \psi_\alpha) + S_\alpha(\psi) \right) f_\phi \right] , \end{aligned} \quad (\text{A.10})$$

where (equations 5 and 6 in the main text)

$$\frac{\partial w^{(n)}}{\partial t} + \langle U_i \rangle \frac{\partial w^{(n)}}{\partial x_i} - \frac{\partial}{\partial x_i} \left[\Gamma_T \frac{\partial w^{(n)}}{\partial x_i} \right] = a^{(n)} , \quad (\text{A.11})$$

$$\frac{\partial s_\alpha^{(n)}}{\partial t} + \langle U_i \rangle \frac{\partial s_\alpha^{(n)}}{\partial x_i} - \frac{\partial}{\partial x_i} \left[\Gamma_T \frac{\partial s_\alpha^{(n)}}{\partial x_i} \right] = b_\alpha^{(n)} , \quad (\text{A.12})$$

and (equations 7 and 12 in the main text)

$$s_\alpha^{(n)} \equiv w^{(n)} \psi_\alpha^{(n)} , \quad (\text{A.13})$$

$$c_{\alpha\beta}^{(n)} \equiv \Gamma_T \frac{\partial \psi_\alpha^{(n)}}{\partial x_i} \frac{\partial \psi_\beta^{(n)}}{\partial x_i} . \quad (\text{A.14})$$

The preceding derivation from the closed joint composition PDF transport equation (A.5) is exact in that, apart from the weighted particle approximation in equation (A.6), no arbitrary choices are made in the derivation of equations (A.11) and (A.12).

The next step is to use equation (A.10) to derive a linear system that matches the number of equations to the $N(K + 1)$ unknown source terms $a^{(n)}$ and $b_\alpha^{(n)}$. The ultimate aim is to solve equations (A.11) and (A.12) to transport the weights and weighted positions of the particle system, using the linear system to determine the source terms $a^{(n)}$ and $b_\alpha^{(n)}$.

The linear system is derived by taking $M = N(K + 1)$ empirical moments of equation (A.10). The empirical moments are defined (equation 8 in the main text)

$$\langle \phi_1^{m_{m1}} \dots \phi_K^{m_{mK}} \rangle_N = \sum_{n=1}^N w^{(n)} \prod_{\alpha=1}^K \psi_\alpha^{(n)m_{m\alpha}} \quad \text{for } m = 1, \dots, M. \quad (\text{A.15})$$

The indices $m_{m\alpha}$ are usually low order non-negative integers. The zeroth and first-order moments are required to ensure that the weights sum to unity and that the empirical means (of any non-reacting scalars) are conserved. The choice of the moment set is otherwise arbitrary. Note however that the linear system may be singular for some moment sets [5] and lower-order moments have been observed to give better conditioning [30].

The linear system may be written as

$$A\alpha = \beta, \quad (\text{A.16})$$

where A is a square $M \times N(K + 1)$ matrix of the form $A = [A_1 \ A_2]$

$$\alpha^\top = [a \ b_1 \ \dots \ b_K], \quad (\text{A.17})$$

$$\beta = A_3 W_3 c + A_2 W_2 r, \quad (\text{A.18})$$

and a and b_α are vectors of length N

$$a^\top = [a^{(1)} \ \dots \ a^{(N)}], \quad (\text{A.19})$$

$$b_\alpha^\top = [b_\alpha^{(1)} \ \dots \ b_\alpha^{(N)}]. \quad (\text{A.20})$$

A_2 and A_3 are $M \times NK$ and $M \times NK^2$ matrices

$$A_2 = [A_{2_1} \ \dots \ A_{2_K}], \quad (\text{A.21})$$

$$A_3 = [A_{3_{11}} \ \dots \ A_{3_{1K}} \ \dots \ A_{3_{K1}} \ \dots \ A_{3_{KK}}], \quad (\text{A.22})$$

and A_1 , A_{2_α} and $A_{3_{\alpha\beta}}$ are $M \times N$ matrices with components defined

$$A_{1,mn} = \left[1 - \sum_{\alpha=1}^K m_{m\alpha} \right] \prod_{\alpha=1}^K \psi_\alpha^{(n)m_{m\alpha}}, \quad (\text{A.23})$$

$$A_{2_{\alpha,mn}} = m_{m\alpha} \psi_\alpha^{(n)m_{m\alpha}-1} \prod_{\substack{\beta=1 \\ \beta \neq \alpha}}^K \psi_\beta^{(n)m_{m\beta}}, \quad (\text{A.24})$$

$$A_{3_{\alpha\beta, mn}} = \begin{cases} m_{m\alpha} \psi_{\alpha}^{(n)m_{m\alpha}-1} m_{m\beta} \psi_{\beta}^{(n)m_{m\beta}-1} \prod_{\substack{\gamma=1 \\ \gamma \neq \beta}}^K \psi_{\gamma}^{(n)m_{m\gamma}} & \text{if } \alpha \neq \beta \\ m_{m\alpha} (m_{m\alpha} - 1) \psi_{\alpha}^{(n)m_{m\alpha}-2} \prod_{\substack{\beta=1 \\ \beta \neq \alpha}}^K \psi_{\beta}^{(n)m_{m\beta}} & \text{otherwise.} \end{cases} \quad (\text{A.25})$$

W_2 and W_3 are $NK \times NK$ and $NK^2 \times NK^2$ diagonal matrices

$$W_2 = \text{diag} [w_1 \cdots w_K] , \quad (\text{A.26})$$

$$W_3 = \text{diag} [w_{11} \cdots w_{1K} \cdots w_{K1} \cdots w_{KK}] , \quad (\text{A.27})$$

and c and r are vectors of length NK^2 and NK

$$c^{\top} = [c_{11} \cdots c_{1K} \cdots c_{K1} \cdots c_{KK}] , \quad (\text{A.28})$$

$$r^{\top} = [r_1 \cdots r_K] , \quad (\text{A.29})$$

where w_{α} , $w_{\alpha\beta}$, $c_{\alpha\beta}$ are r_{α} are vectors of length N with components defined

$$w_{\alpha}^{\top} = w_{\alpha\beta}^{\top} = [w^{(1)} \cdots w^{(N)}] , \quad (\text{A.30})$$

$$c_{\alpha\beta}^{\top} = [c_{\alpha\beta}^{(1)} \cdots c_{\alpha\beta}^{(N)}] , \quad (\text{A.31})$$

$$r_{\alpha}^{\top} = [r_{\alpha}^{(1)} \cdots r_{\alpha}^{(N)}] , \quad (\text{A.32})$$

and (equation 13 in the main text)

$$r_{\alpha}^{(n)} = \frac{C_{\phi}}{2\tau_{\phi}} (\langle \phi_{\alpha} \rangle_N - \psi_{\alpha}^{(n)}) + S_{\alpha}(\psi^{(n)}) . \quad (\text{A.33})$$

The final step in the derivation forces the M empirical moments of the transported particle system to obey the equivalent moment transport equation that could be derived directly from the closed joint composition PDF transport equation (A.5).

A.2 DQMoM-IEM

The DQMoM derivation can be modified to implement DQMoM-IEM by setting $a^{(n)} = 0$ in equations (A.10) and (A.11) and evaluating $b_{\alpha}^{(n)}$ by solving a modified linear system

$$A_2 [b_1 \cdots b_K]^{\top} = \beta , \quad (\text{A.34})$$

where equation (A.34) is derived by taking $M = NK$ unmixed empirical moments of equation (A.10). The zeroth moment is no longer required because the source term for the weights is null. A_2 and β are defined as previously.

Equation (A.34) is equivalent to equation (11) given in the main text.

B Method of moments implementation

This section describes the implementation of an inert method of moments solution of the closed joint composition PDF transport equation (1).

A transport equation for the moments λ of the joint composition PDF is derived by taking moments of equation (1)

$$\frac{\partial \lambda}{\partial t} + \langle U_i \rangle \frac{\partial \lambda}{\partial x_i} - \frac{\partial}{\partial x_i} \left[\Gamma_T \frac{\partial \lambda}{\partial x_i} \right] = R_\lambda. \quad (\text{B.1})$$

In the inert case, the chemical source term in equation (1) is null $S_\alpha = 0$. The source term R_λ is found by taking the moments of the micromixing term and integrating by parts

$$R_{\lambda_{m_1, \dots, m_K}} = \int \dots \int_{-\infty}^{+\infty} \prod_{\beta=1}^K \psi_\beta^{m_\beta} \left(-\frac{\partial}{\partial \psi_\alpha} \left[\frac{C_\phi}{2\tau_\phi} (\langle \phi_\alpha \rangle - \psi_\alpha) f_\phi \right] \right) d\psi_1 \dots d\psi_K$$

such that

$$\begin{aligned} R_{\lambda_{m_1, \dots, m_K}} &= \frac{C_\phi}{2\tau_\phi} \sum_{\alpha=1}^K \int \dots \int_{-\infty}^{+\infty} m_\alpha \psi_\alpha^{-1} \prod_{\beta=1}^K \psi_\beta^{m_\beta} (\langle \phi_\alpha \rangle - \psi_\alpha) f_\phi d\psi_\alpha \prod_{\substack{\beta=1 \\ \beta \neq \alpha}}^K d\psi_\beta \\ &\quad - \underbrace{\frac{C_\phi}{2\tau_\phi} \sum_{\alpha=1}^K \int \dots \int_{-\infty}^{+\infty} \left[\prod_{\beta=1}^K \psi_\beta^{m_\beta} (\langle \phi_\alpha \rangle - \psi_\alpha) f_\phi \right]_{\psi_\alpha=-\infty}^{\psi_\alpha=\infty} \prod_{\substack{\beta=1 \\ \beta \neq \alpha}}^K d\psi_\beta}_{=0} \\ &= \frac{C_\phi}{2\tau_\phi} \left[m_1 (\lambda_{1,0,\dots,0} \lambda_{m_1-1,m_2,\dots,m_K} - \lambda_{m_1,m_2,\dots,m_K}) \right. \\ &\quad + m_2 (\lambda_{0,1,\dots,0} \lambda_{m_1,m_2-1,\dots,m_K} - \lambda_{m_1,m_2,\dots,m_K}) \\ &\quad \vdots \\ &\quad \left. + m_K (\lambda_{0,0,\dots,1} \lambda_{m_1,m_2,\dots,m_K-1} - \lambda_{m_1,m_2,\dots,m_K}) \right], \end{aligned} \quad (\text{B.2})$$

where the summation of the underbraced term to zero follows directly from consideration of the values taken by the PDF f_ϕ and the source term $(\langle \phi_\alpha \rangle - \psi_\alpha)$ at the limits.

Equation (B.1) is solved for the λ_1 , λ_2 , λ_3 and λ_4 unmixed moments of each scalar using the operator splitting described in Section 3.1. The operators are defined

$$\begin{aligned} \mathcal{F}_1(\lambda) &= R_\lambda, \\ \mathcal{F}_2(\lambda) &= -\langle U_i \rangle \frac{\partial \lambda}{\partial x_i} + \frac{\partial}{\partial x_i} \left[\Gamma_T \frac{\partial \lambda}{\partial x_i} \right]. \end{aligned}$$

The first operator $\mathcal{F}_1(\lambda)$ may be integrated either analytically or using RADAU5. Both methods were implemented for the purpose of this work. Both were observed to give identical results, with the obvious caveat that the analytic implementation was much faster.